TARGET LITHOLOGY AS A CONTROL ON CRATER RIM THERMAL INERTIA VARIABILITY IN LOW SURFACE DUST COVER AREAS ON MARS: APPLICATIONS OF SECONDARY CRATER POPULATIONS. Helle L. Skjetne[1] and Jeffrey E. Moersch[1], [1]Department of Earth and Planetary Sciences, University of Tennessee, Knoxville; 1621 Cumberland Avenue, 602 Strong Hall, Knoxville, TN 37996-1526, USA (hskjetne@vols.utk.edu).

Summary: Neighboring impact craters of similar size and target lithology in low dust cover regions on Mars exhibit variations in thermal inertia (TI) on their rims [e.g., 1–3]. Although crater age has been shown to be a factor in controlling crater rim TI [3], secondary crater populations (i.e., crater fields formed by the ejecta from an initial primary impact event) covering more than one lithologic unit are useful in in determining whether target lithology also plays a role because these craters form nearly simultaneously. We find that rim TI within one population of secondaries spanning two lithologic units in Hesperia Planum (*Fig. 1a*) appear to display a relationship between target lithology and rim TI: secondary crater rims in the older unit (middle Noachian highland, mNh) appear less pristine and have lower TI values compared to rims in the adjacent younger unit (early Hesperian volcanic, eHv). Comparison across a larger set of secondary crater populations that straddle lithologic units will provide further constraints on the factors responsible for crater rim TI variability.

Background: Rims of primary impact craters of similar size and potentially very different ages have been shown to range between 160 to 600 J m^{-2} K^{-1} $s^{-1/2}$ (unit of TI; tiu) within a single TI scene [2,3], which suggests that there are underlying mechanisms responsible for this variance. TI is an expression of how readily the temperature of a material responds to a time-varying energy flux (i.e., heat source, usually insolation) in the upper few centimeters of the surface. It is defined as TI = $(k\rho c)^{1/2}$, where k is thermal conductivity, ρ is bulk density, and c is the specific heat capacity of the surface material [1,4]. For rock and regolith material, TI is primarily controlled by k, which is dominated by variations in grain size [5–8]. Generally, lower TI corresponds to fine-grained surfaces whereas higher TI values corresponds to coarser grained and/or indurated surfaces (e.g., dust to fine sand: <20–250 tiu, med. sand to coarse sand: 250–523 tiu, pebbles and larger: 523–900 tiu) [1,8]. Previous TI investigations of primary crater rims in low-dust cover areas on Mars interpreted TI variability to be a function of rim degradation producing fine-grained regolith (e.g., comminution) [3].

Objectives: While previous studies [2,3] suggested that degradation state and relative crater ages are primarily responsible for observed TI variations, other factors may be at work. In this study, we eliminate age as a variable by studying rim TI values of individual secondary craters (formed by fragments ejected during a primary impact event [e.g., 9]) that straddle lithologic units in low dust cover regions on Mars [e.g., 10]. Such populations of craters (e.g., *Fig. 1a*) are useful in understanding variations in rim TI because all members of the same population of secondaries form essentially contemporaneously [8], eliminating crater age as a factor in accounting for variations. Secondary craters within one population are first recognizable beyond the edge of the continuous ejecta blanket [9] and are generally discernable up to tens to hundreds of crater radii away (i.e., hundreds to thousands of kilometers away) from the primary impact site [e.g., 11–13]. The large spatial range of secondary craters makes it more likely that they cover more than one lithologic unit, and can therefore be used to assess the effects of target lithologic properties. This project presents preliminary data from one secondary crater population that will be further refined and expanded upon with other secondary crater populations in ongoing work.

Data and Methods: For this preliminary study we used a population of secondaries associated with a 75-km-diameter unnamed primary crater centered at 13.7°S, 113.4°E in the southern highlands of Mars (*Fig. 1a*). This crater has an Amazonian/Hesperian age (AHi) and is located on the boundary between the Hesperia Planum lava plains and the heavily cratered region Terra Cimmeria [14]. The secondary crater population associated with this impact crater is suited for our study because it exhibits: 1) limited dust cover (Dust Cover Index, DCI < 0.97–0.99) [10], 2) relatively low differences in topographic relief [14,15], and 3) the prominent population of secondary craters, straddling both eHv units and mNh units [14]. We will extend our work globally to other selected populations of secondaries that are in areas that meet the same criteria and explore radial trends within each unit. To explore effects of crater age and type, we will also measure rim TI of primary craters within each impact ejecta field.

We used ~5 m px^{-1} Context Camera (CTX) images [16] to obtain morphometric secondary crater rim measurements and 100 m px^{-1} THermal EMission Imaging System (THEMIS) derived TI images [7] to extract average rim TI values. We traced the rims by visual inspection using manually selected, closely spaced sampling points from locations that can be

identified confidently to represent each crater rim. Only secondary craters ≥1 km diameter displaying typical secondary characteristics (e.g., v-shaped ejecta, clusters or chains, and elongation in the direction radial to the primary) with the highest likelihood of originating from the parent primary crater of interest are included in our final dataset. TI data were extracted from the identified rim traces per the methods described in [2,3] and averaged TI values were found for each secondary crater using Microsoft Excel. The populations of these rim TI values were analyzed in the statistical language R.

Results and Observations: We extracted rim TI values of 182 secondary craters within a secondary crater population. Mapped secondary crater rim TI values in this area typically measure between ~155 to 281 J m^{-2} K^{-1} $s^{-1/2}$ (*Fig. 1b*). Generally, secondaries in the older mNh unit visually appear more degraded compared to those in the eHv unit, and measured rim TI values appear to be slightly lower than in the eHv unit. We used Welch's t-test to compare means between the secondaries on the two units (see *Fig. 1b*) and found a corresponding p-value of 0.0003915. Since this p-value is <0.05, we find a statistically significant difference in rim TI values for secondaries on the two units.

Conclusions and Future work: Based on an initial analysis of crater rim TI measurements from one population of secondary craters spanning two lithologic units (*Fig. 1a*), a relationship between rim TI and target lithology appears to be present. We hypothesize that target unit lithologic properties (e.g., composition, susceptibility to degradation) contribute to variations in crater rim TI across regions on Mars with low dust cover. If this relationship holds when other populations of secondary craters are examined, it would suggest that differences in crater rim TI are not only caused by the age of the crater [3] but also pre-existing target lithology differences. If proven, this hypothesis would be useful because knowledge of relative rates of degradation is of fundamental utility for surface age dating on Mars and other solid bodies [9]. We anticipate that upcoming results from a larger sample set of secondary crater populations across a range of terrains will provide further constraints on sources of crater rim TI variation and relative degradation rates across Mars.

Acknowledgements: This work was supported by THEMIS subcontract from Arizona State University to the University of Tennessee (#10-254).

References: [1] Mellon M.T. et al. (2000) *Icarus*, *148*, 437–455. [2] Beddingfield C.B. et al. (2018) *Icarus*, *314*, 345–363. [3] Beddingfield C.B. et al. (2021) *Icarus*, *370*, 114678. [4] Palluconi F.D. and Kieffer H.H. (1980) *Icarus*, *45*, 415–426. [5] Kieffer H.H. et al. (1973) *JGR*, *78(20)*, 4291–4312. [6] Presley M.A. and Christensen P.R. (1997) *JGR*, *102(E3)*, 6551–6566. [7] Fergason R.L. et al. (2006) *JGR*, *111*, E12004. [8] Putzig N.E. and Mellon M.T. (2007) *Icarus*, *1*, 68–94. [9] Melosh H.J. (1989) *Oxford U. Press NY*. [10] Ruff S.W. and Christensen P.R. (2002) *JGR*, *107*. [11] Tornabene L.L. et al. (2006) *JGR: Planets*, *111*, *E10*. [12] Robbins S.J. and Hynek B.M. (2011) *JGR*, *116*, E10003. [13] Housen K.R. and Holsapple K.A. (2011) *Icarus*, *211*, 856–875. [14] Tanaka K.L. et al. (2014) *Planet. and Space Sci.*, *95*, 11–24. [15] Fassett C.I. and Thomson B.J. (2014) *JGR: Planets*, *119*, *10*, 2255–2271. [16] Dickson J.L. et al., (2018) *LPSC*, *2083*.

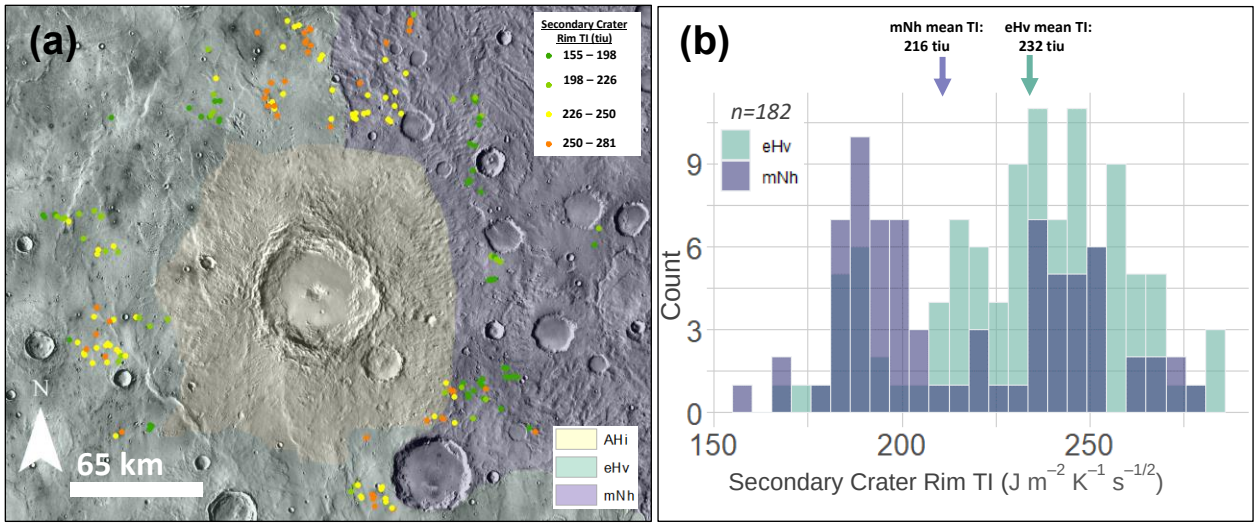

Figure 1: Example of secondary crater rim TI variations in early Hesperian volcanic (eHv; green) and middle Noachian highland (mNh; purple) target units. *(a) Amazonian/Hesperian unnamed crater (AHi; yellow) centered at 13.7°S 113.4°E, shown in THEMIS daytime-IR mosaics (100 m* px^{-1}*) compared to regional geologic units [14]. Rim TI values extracted from quantitative THEMIS-derived TI scenes [7] are shown for each mapped secondary crater. (b) Histogram of secondary crater rim TI from preliminary mapping results (note overlap).*